

# Universal properties of penetrative turbulent Rayleigh–Bénard convection in cold water near 4°C

Qi Wang<sup>1,2</sup>, Philipp Reiter<sup>3</sup>, Detlef Lohse<sup>1,3,\*</sup> and Olga Shishkina<sup>3†</sup>

<sup>1</sup>*Physics of Fluids Group and Max Planck Center for Complex Fluid Dynamics,*

*MESA+ Institute and J. M. Burgers Centre for Fluid Dynamics,*

*University of Twente, P.O. Box 217, 7500AE Enschede, The Netherlands*

<sup>2</sup>*Department of Modern Mechanics, University of*

*Science and Technology of China, Hefei 230027, China*

<sup>3</sup>*Max Planck Institute for Dynamics and Self-Organization, 37077 Göttingen, Germany*

(Dated: November 15, 2021)

## Abstract

Penetrative turbulence, which occurs in a convectively unstable fluid layer and penetrates into an adjacent, originally stably stratified layer, is numerically and theoretically analyzed. We chose the most relevant example, namely thermally driven flow of water with a temperature around  $T_m \approx 4^\circ\text{C}$ , where it has its density maximum. We pick the Rayleigh–Bénard geometry with the bottom plate temperature  $T_b > 4^\circ\text{C}$  and the top plate temperature  $T_t \leq 4^\circ\text{C}$ . Next to the overall thermal driving strength set by the temperature difference  $\Delta = T_b - T_t$  (the Rayleigh number  $Ra$  in dimensionless form), the crucial new control parameter as compared to standard Rayleigh–Bénard convection is the density inversion parameter  $\theta_m \equiv (T_m - T_t)/\Delta$ . The crucial response parameters are the relative mean mid-height temperature  $\theta_c$  and the overall heat transfer (i.e., the Nusselt number  $Nu$ ). We theoretically derive the universal (i.e.,  $Ra$ -independent) dependence  $\theta_c(\theta_m) = (1 + \theta_m^2)/2$ , which holds for  $\theta_m$  below a  $Ra$ -dependent critical value, beyond which  $\theta_c(\theta_m)$  sharply decreases and drops down to  $\theta_c = 1/2$  at  $\theta_m = \theta_{m,c}$ . Our direct numerical simulations with  $Ra$  up to  $10^{10}$  are consistent with these results. The critical density inversion parameter  $\theta_{m,c}$  can be precisely predicted by a linear stability analysis. The heat flux  $Nu(\theta_m)$  monotonically decreases with increasing  $\theta_m$  and we can theoretically derive a universal relation for the relative heat flux  $Nu(\theta_m)/Nu(0)$ . Finally, we numerically identify and discuss rare transitions between different turbulent flow states for large  $\theta_m$ .

---

\* [d.lohse@utwente.nl](mailto:d.lohse@utwente.nl)

† [Olga.Shishkina@ds.mpg.de](mailto:Olga.Shishkina@ds.mpg.de)

Turbulent Rayleigh–Bénard convection (RBC) [1–3], which occurs in a fluid layer due to a temperature difference at its bottom and top surfaces, is the paradigmatic model system to study thermally driven turbulence. Usually it is considered within the Oberbeck–Boussinesq (OB) approximation, in which all fluid properties are assumed to be constant, apart from the density in the buoyancy term of the momentum equation, where it is assumed to be linearly dependent on the temperature. However, in many cases in nature and technology, the density of many fluids is strongly non-linear and even non-monotonic with the temperature, which significantly influences the flow patterns and the heat transport properties in the system. The most famous and relevant example is water, for which the density is maximal at  $T_m \approx 4^\circ\text{C}$ . This density maximum has a drastic influence on many natural phenomena like the freezing of lakes and estuaries, and the survival of fauna in shallow waters in winter [4–7]. However, also here RBC can be used again as paradigmatic model system, but now correspondingly RBC of cold water near  $T_m$ . This is an example of so-called penetrative convection [8, 9], where convection in a thermally unstable layer penetrates into the adjacent stable layers. Penetrative convection is not only important for water around  $4^\circ\text{C}$  and freezing lakes etc., but also in many astrophysical settings, for example, in the tachocline of the Sun [10], and possibly in the liquid core of the Earth [11] and in the Jupiter’s atmosphere [12].

The control parameters in this problem are the Prandtl number  $Pr \equiv \nu/\kappa$ , where  $\nu$  is the kinematic viscosity and  $\kappa$  the thermal diffusivity of the fluid, the aspect ratio  $\Gamma \equiv W/H$  as ratio of the width  $W$  and the height  $H$  of the domain, and the Rayleigh number  $Ra \equiv g\alpha\Delta^q H^3/\nu\kappa$ , where  $H$  is the height of the cell and  $g$  the gravitational acceleration. Note that the nonlinear dependence of  $Ra$  on the temperature difference  $\Delta \equiv T_b - T_t$  between the hot bottom plate temperature  $T_b > T_m$  and the cold top plate temperature  $T_t \leq T_m$  reflects the nonlinear relationship between the density and the temperature around the density maximum, namely  $\rho = \rho_m(1 - \alpha|T - T_m|^q)$  [13], where  $\rho_m \approx 1000\text{kg}/\text{m}^3$  is the maximum density at the temperature  $T_m \approx 4^\circ\text{C}$ . Here we take the measured material properties for water, namely  $q = 1.895$  and  $\alpha = 9.30 \times 10^{-6}(\text{K})^{-q}$  as isobaric thermal expansion coefficient. Apart from the density, all other material properties of the fluid are assumed to be constant. The crucial new control parameter in penetrative convection as compared to standard RBC is the density inversion parameter  $\theta_m \equiv (T_m - T_t)/\Delta$ . We consider  $0 \leq \theta_m < 1$ , with the limiting case  $\theta_m = 0$  (or  $T_t = T_m$ ) without a stably stratified region and thus being closest to standard RBC and the other limiting case  $\theta_m = 1$  (or  $T_b = T_m$ ) being fully stably stratified.

The response parameters of the system are the Nusselt number  $Nu \equiv QH/(k\Delta)$  and the Reynolds number  $Re \equiv UH/\nu$ , which indicate the non-dimensional heat transport and flow

strength in the system, respectively. Here  $Q$  is the heat flux crossing the system,  $k$  the thermal conductivity, and  $U \equiv \langle \mathbf{u}^2 \rangle_{V,t}^{1/2}$  the time and volume averaged root-mean-square velocity of the flow. The central new response parameter in penetrative convection as compared to standard RBC is the mean temperature  $T_c$  at mid height, or, when non-dimensionalized,  $\theta_c = (T_c - T_t)/\Delta$ . Whereas in standard RBC  $\theta_c = 1/2$  for symmetry reasons, here in penetrative convection  $1/2 \leq \theta_c \leq 1$ , reflecting that the hot fluid from the bottom unstably stratified region can more easily reach the center than the cold fluid from top stably stratified region.

Early studies of penetrative RBC focused on the stability of the flows near the onset of convection [8, 9, 14–16]. Recently, turbulent RBC of cold water near  $T_m$  also attracted attention [7, 17, 18]. In Ref. [17], the internal gravity wave excitation by convection was studied using two-dimensional (2D) direct numerical simulations (DNS). In Ref. [18], convection in cold water was investigated by means of 2D and three-dimensional (3D) DNS. It was shown that for  $0 \leq \theta_m \lesssim 0.9$ , the mean central temperature  $\theta_c$ , the normalized Nusselt number  $Nu(\theta_m)/Nu(0)$ , and the normalized Reynolds number  $Re(\theta)/Re(0)$  are almost independent of  $Ra$  and thus to be claimed to be universal.

However, in this study we will show that when extending the range of the control parameter  $\theta_m$  towards 1 (i.e., towards the fully stably stratified case), the center temperature  $\theta_c$  strongly depends on  $Ra$ . Moreover, we propose a model for the dependence of this key response parameter  $\theta_c$  on the density inversion parameter  $\theta_m$  and demonstrate its excellent agreement with the DNS data. Also the dependence of the other central response parameter, namely the Nusselt number, on  $\theta_m$  is theoretically explained.

The flow dynamics is governed by the incompressibility condition  $\nabla \cdot \mathbf{u} = 0$  and the Navier-Stokes equation with (nonlinear, see above) buoyancy forcing and the advection diffusion equation,

$$\partial \mathbf{u} / \partial t + \mathbf{u} \cdot \nabla \mathbf{u} = \sqrt{Pr/Ra} \nabla^2 \mathbf{u} - \nabla p + |\theta - \theta_m|^q \vec{e}_z, \quad (1)$$

$$\partial \theta / \partial t + \mathbf{u} \cdot \nabla \theta = 1/\sqrt{RaPr} \nabla^2 \theta, \quad (2)$$

where  $\mathbf{u} = (u, w)$ ,  $\theta$ , and  $p$  are the velocity, temperature, and pressure, respectively. For non-dimensionalization, we choose  $H$  and  $U_f = (g\alpha\Delta^q H)^{1/2}$  as the reference length and velocity. The reference time is free-fall time  $t_f = H/U_f$ . Temperature is nondimensionalized as  $\theta = (T - T_t)/\Delta$ . We consider periodic boundary conditions (BCs) in the horizontal direction and no-slip isothermal BCs at the top and bottom boundaries.

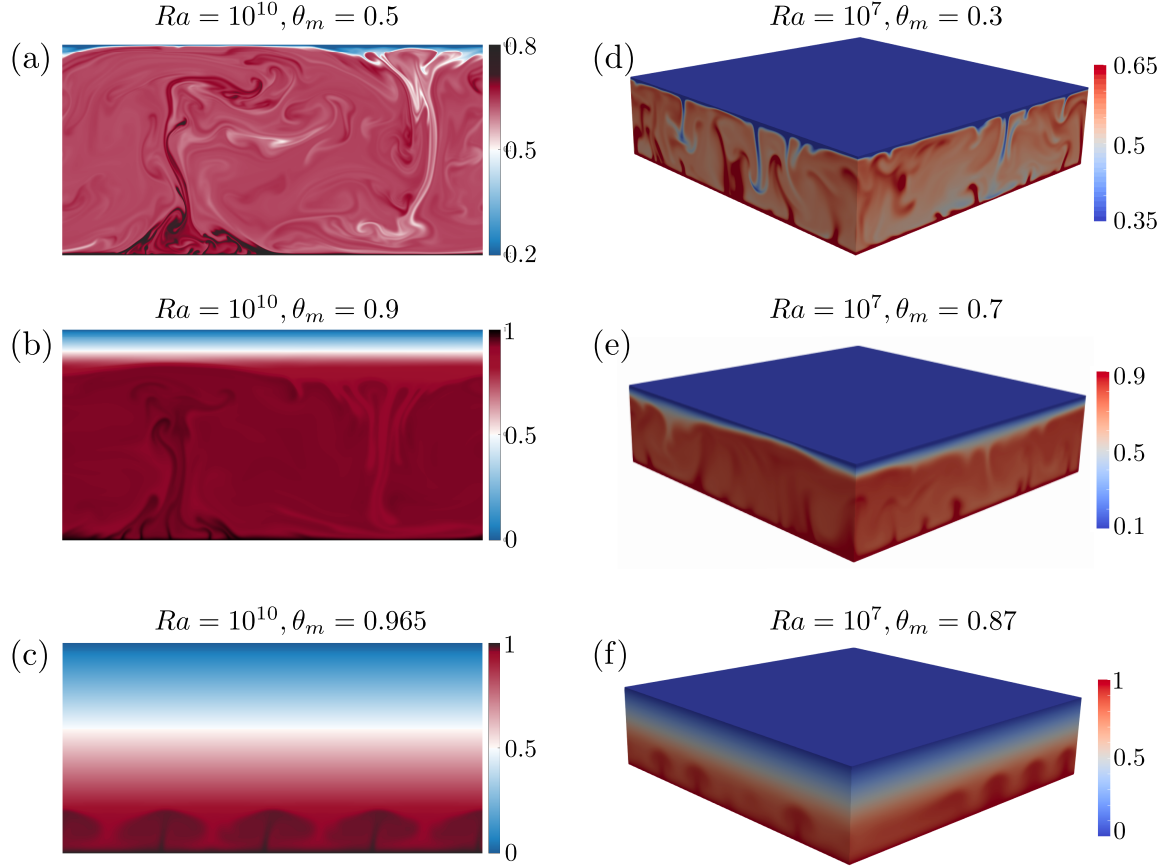


FIG. 1. Instantaneous temperature fields for different  $\theta_m$  in (a–c) 2D DNS for  $Ra = 10^{10}$  and  $\Gamma = 2$  and (d–f) 3D DNS for  $Ra = 10^7$  and  $\Gamma = 4$ : (a)  $\theta_m = 0.5$ , (b)  $\theta_m = 0.9$ , (c)  $\theta_m = 0.965$ , (d)  $\theta_m = 0.3$ , (e)  $\theta_m = 0.7$ , and (f)  $\theta_m = 0.87$ .

We perform 2D DNS in a broad  $Ra$ -range,  $10^7 \leq Ra \leq 10^{10}$ , with fixed aspect ratio  $\Gamma = 2$ .  $Pr$  is fixed to 11.57 in all simulations, which corresponds to the value for water at  $4^\circ\text{C}$ . In addition, we perform 3D DNS for  $Ra = 10^7$  and  $\Gamma = 4$ . The governing equations are solved with the second-order finite-difference code AFiD [19, 20], which has already been extensively used to study RBC, see, e.g., [21, 22]. The used staggered grids satisfy the resolution requirements for DNS [23]. Details on the simulations can be found in the Supplementary materials.

Fig. 1 gives the reader an idea of the flow organization. Figs. 1(a–c) show 2D instantaneous temperature fields for different  $\theta_m$  and  $Ra = 10^{10}$ . For  $\theta_m > 0$ , only the lower layer in the cell can be convectively unstable. For not too large  $\theta_m$ , convection penetrates from the lower layer into the upper, gravitationally stable, layer, and this increases the bulk temperature. For  $\theta_m = 0.5$  (Fig. 1 a), the convective flow occupies almost the whole domain, while for  $\theta_m = 0.9$  (Fig. 1 b)

a stably stratified layer forms near the top plate. For even larger  $\theta_m = 0.965$  (Fig. 1 c), the flow stratification takes place nearly in the whole cell. A similar change of the global flow structure with increasing  $\theta_m$  is observed in the 3D DNS (Figs. 1 d–f).

The intrusion of penetrating convection from the convectively unstable regions to convectively stable ones resembles those observed in internally heated convection [24–26] and horizontal convection [27–29], as well as in counter-rotating Taylor–Couette flows, where stratified angular velocity zones are located near the outer cylinder [30–32].

The time- and area-averaged temperature profiles and their dependences on  $\theta_m$  for  $Ra = 10^{10}$  are presented in Fig. 2(a). It shows that for  $\theta_m = 0$ , the profile is similar to that in the OB case, with the mean central temperature  $\theta_c$  being close to the arithmetic mean of the top and bottom temperatures ( $\theta_c = 1/2$ ). One can see that with increasing  $\theta_m$ , the temperature in the thermally unstable, lower zone gradually increases. However, the mean temperature  $\theta_c$  at mid-height behaves non-monotonically. With increasing  $\theta_m$ , it first increases as long as the half height location ( $z/H = 0.5$ ) lies in the thermally unstable region, but then it starts to decrease back to the arithmetic mean of the top and bottom temperatures, once the mid-height location is swallowed up by the upper stably stratified region.

Fig. 2(b) further shows the mean central temperature  $\theta_c$  as function of  $\theta_m$ , for both the 2D and the 3D cases. We note that the collapse of the 3D data with the 2D data confirms the similarity between 2D and 3D RBC for large  $Pr$  [33]. One can observe two different regimes: in regime I, for low density inversion parameter  $0 \leq \theta_m \ll 1$ , the central temperature  $\theta_c$  monotonically increases with increasing  $\theta_m$ , and all the data collapse onto a single curve, independently of  $Ra$ . However, in regime II, for  $\theta_m$  close to 1, with increasing  $\theta_m$  the central temperature  $\theta_c$  extremely sharply drops to the value  $1/2$ . We denote the value of  $\theta_m$ , at which  $\theta_c$  reaches  $1/2$  in regime II, as  $\theta_{m,c}$ , i.e.,  $\theta_c(\theta = \theta_{m,c}) = 1/2$ . It is clear that  $\theta_{m,c}$  increases with increasing  $Ra$  and approaches 1 for  $Ra \rightarrow \infty$ , implying that for strong enough thermal driving the whole cell is filled with penetrative turbulence, even for large density inversion parameter close to 1.

We now set out to theoretically explain the universal dependence of the central temperature  $\theta_c$  on the control parameter  $\theta_m$  in regime I. First we notice that for  $\theta_m = 0$ , the temperature of the fluid is larger than  $T_m$  through the entire convection cell and therefore the situation is similar to the OB case. Thus, the central temperature can be well approximated by the arithmetic mean of the top and bottom temperatures, i.e.,  $\theta_c = 1/2$ . With increasing  $\theta_m$ , the height, at which the time- and area-averaged temperature equals  $T_m$ , gradually decreases from the top towards the bottom, and at

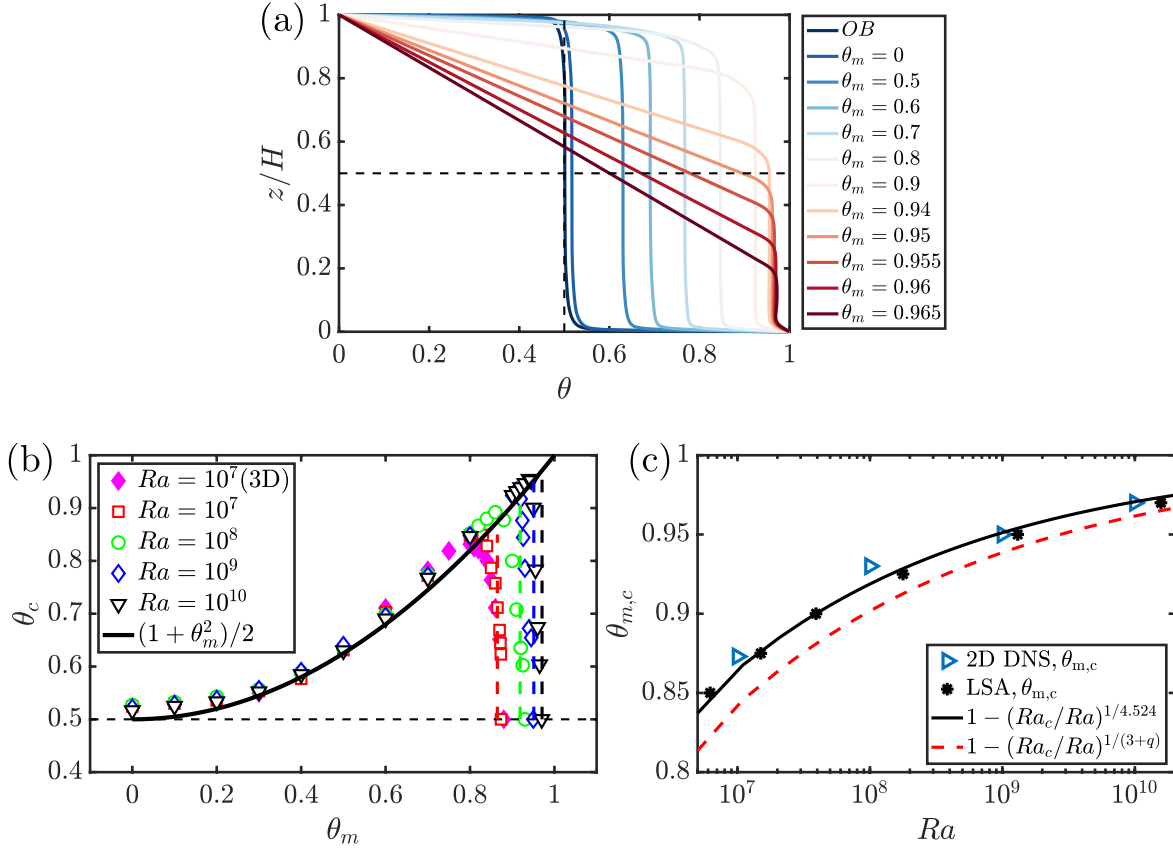


FIG. 2. (a) Time- and horizontally averaged temperature profiles for different  $\theta_m$ , as obtained in the 2D DNS for  $Ra = 10^{10}$  and  $\Gamma = 2$ . (b) Time- and horizontally averaged temperature at mid-height,  $\theta_c$ , as function of  $\theta_m$ , in the 2D (open symbols) and 3D (closed symbols) cases for different  $Ra$ . The solid line shows the theoretical prediction  $\theta_c = (1 + \theta_m^2)/2$ , which is universal for all  $Ra$ . Predictions of the linear stability analysis for the critical  $\theta_m = \theta_{m,c}$ , where  $\theta_c$  drops back to  $1/2$ , depend on  $Ra$  and are shown with the dashed vertical lines of the colors that correspond to the DNS data. (c) The critical  $\theta_{m,c}$  versus  $Ra$ , as obtained from the 2D DNS (open symbols), linear stability analysis (closed symbols and their fit shown with the solid line) and from the theoretical model  $\theta_{m,c} = 1 - (Ra_c/Ra)^{1/(3+q)}$ , with  $Ra_c = 1171$  and  $q = 1.895$  (dashed line).

a certain moment arrives at the mid-height, which indicates the end of regime I. Therefore, when  $\theta_m \rightarrow 1$  within regime I, the central temperature  $\theta_c$  tends to  $\theta_m$  and  $\lim_{\theta_m \rightarrow 1} \frac{1-\theta_c}{1-\theta_m} = 1$ . Applying L'Hôpital's rule to this limit, we obtain that  $\lim_{\theta_m \rightarrow 1} \frac{d\theta_c}{d\theta_m} = 1$ . Thus, for  $\theta_m \rightarrow 1$ , one can take  $\theta_c = \theta_m$  and  $d\theta_c/d\theta_m = 1$ . This together with  $\theta_c = 1/2$  at  $\theta_m = 0$  gives a simple polynomial

approximation of the mean central temperature within the regime I,

$$\theta_c = (1 + \theta_m^2)/2. \quad (3)$$

Fig. 2(b) demonstrates that the model (3) accurately represents the 2D and 3D DNS data within regime I.

Next we will explain the abrupt drop of the central temperature near  $\theta_{m,c}$  as function of  $Ra$ . Therefore, for any given  $Ra$ , we must find  $\theta_m = \theta_{m,c}$ , at which the central temperature  $\theta_c$  drops back to  $1/2$  in regime II, see Fig. 2(b). As discussed above, the lower layer of the cell is convectively unstable for small  $\theta_m$ . However, the situation changes dramatically for larger  $\theta_m$ , when the Rayleigh number  $Ra_\ell$  associated with this layer becomes as small as the critical Rayleigh number  $Ra_c$  for the onset of convection in a domain with no-slip BCs at its lower surface and free-slip BCs at its top surface, at which the temperature is kept equal to  $T_m$ . When at a certain  $\theta_m = \theta_{m,c}$  the value of  $Ra_\ell$  becomes equal to  $Ra_c$ , the lower layer becomes convectively stable and stratified as the upper layer, and therefore the central temperature in the whole cell becomes equal to the arithmetic mean of the top and bottom temperatures of the cell, i.e.,  $\theta_c = 1/2$ .

The Rayleigh number  $Ra_\ell$  associated with such stratified lower layer is related to  $Ra$  as  $Ra_\ell = (1 - \theta_{m,c})^{3+q}Ra$ . This is due to the reduction of the height of the layer to  $(1 - \theta_{m,c})H$ , compared to the height  $H$  of the whole cell, and due to the reduction of the temperature difference between the boundaries of the layer to  $(1 - \theta_{m,c})\Delta$ , compared to the temperature difference  $\Delta$  at the cell plates. Equating  $Ra_\ell = Ra_c$ , we obtain the prediction

$$\theta_{m,c} = 1 - (Ra_c/Ra)^{1/(3+q)}. \quad (4)$$

The critical  $Ra_c$  for the onset of convection in an infinite layer of cold water with the top temperature  $T_m$ , no-slip BCs at the bottom and free-slip BCs at the top equals  $Ra_c = 1171$ , as we calculated using linear stability analysis (LSA), see also Supplementary materials for more information. The results produced by the model (4) are plotted as dashed line in Fig. 2(c). The model prediction for the behaviour of  $\theta_{m,c}$  as function of  $Ra$  is consistent with the DNS results (open symbols).

Even more accurate predictions of  $\theta_{m,c}$  can be obtained with the LSA applied to a 2D convection cell filled with cold water, for the cell aspect ratio  $\Gamma = 2$ , and periodic BC at the side walls. Thus, for any given  $\theta_m = \theta_{m,c}$ , the LSA provides the critical Rayleigh number  $Ra$  for the onset of convection; a relation between them is very precisely described by  $\theta_{m,c} = 1 - (1171/Ra)^{1/4.524}$ , see the Supplementary material. These predictions by the LSA are in a very good agreement with the DNS data, as it can be seen in Fig. 2(c).

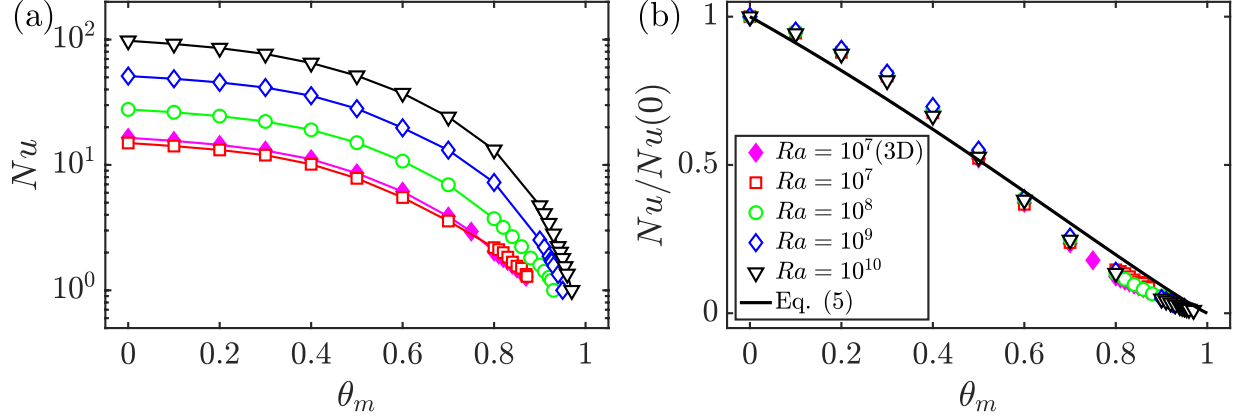


FIG. 3. Nusselt numbers  $Nu$  as function of the density inversion parameter  $\theta_m$  for different  $Ra$ : (a) Absolute values from the DNS (lines to guide the eye) and (b) normalized with the values at  $\theta_m = 0$ . The line shows the theoretical model, Eq. (5).

We now focus on how the Nusselt number  $Nu$  depends on the control parameter  $\theta_m$  and develop a model for the reduced Nusselt number,  $Nu(\theta_m)/Nu(\theta_m = 0)$ , based on our knowledge on the heat transport properties in the OB case. Fig. 3(a) shows that for all  $Ra$ , the absolute values of  $Nu(\theta_m)$  monotonically decrease with growing  $\theta_m$ . After normalization using  $Nu(\theta_m = 0)$ , the data well collapse onto a single curve, as shown in Fig. 3(b).

How to account for this universal relationship? For  $\theta_m = 0$ , the whole RBC cell can be considered as an almost OB one, which is characterized by  $Ra$  and the corresponding critical Rayleigh number  $Ra_{c,0}$  for the onset of convection in this cell. For  $\theta_m > 0$ , only the lower layer can be treated as an OB cell. The temperature at this layer's upper surface is  $T_m$  and the corresponding Rayleigh number and critical Rayleigh number are  $Ra_\ell$  and  $Ra_c$ , respectively. From 2D OB DNS with  $Pr = 10$  [21] we know that in the considered  $Ra$ -range,  $Nu$  scales as  $(Ra/Ra_{c,0})^\gamma$  with  $\gamma \approx 0.27$ . Therefore  $Nu(\theta_m)/Nu(0) = (Ra_\ell/Ra_c)^\gamma (Ra_{c,0}/Ra)^\gamma = (Ra_\ell/Ra)^\gamma (Ra_{c,0}/Ra_c)^\gamma$ . Due to the reduced height and the temperature drop in the lower layer compared to the whole RBC cell (by almost  $(1 - \theta_m)$ , as a first approximation), the value of  $Ra_\ell/Ra$  can be approximated as  $(1 - \theta_m)^4$ . The critical Rayleigh numbers for the onset of convection can be approximated as  $Ra_c \sim [1 + (1 - \theta_m)^2/\Gamma^2]^2$  and  $Ra_{c,0} \sim [1 + 1/\Gamma^2]^2$  (see more information in the Supplementary material), which altogether lead to

$$\frac{Nu(\theta_m)}{Nu(0)} \approx \left[ \frac{(1 + \Gamma^2)(1 - \theta_m)^2}{\Gamma^2 + (1 - \theta_m)^2} \right]^{2\gamma} = \left[ \frac{5(1 - \theta_m)^2}{4 + (1 - \theta_m)^2} \right]^{0.54}. \quad (5)$$

This prediction is consistent with the general trend of the normalized Nusselt number, as can be



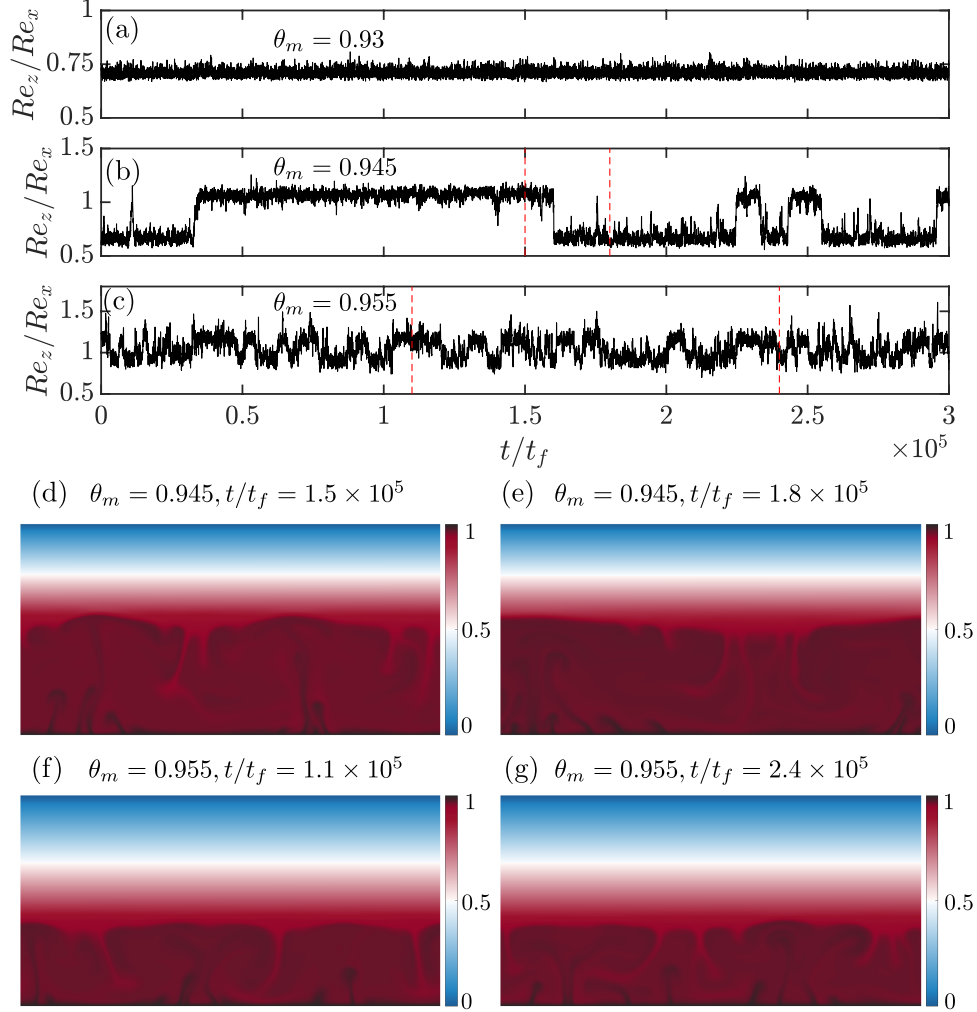


FIG. 4. (a–c) Time evolution of the Reynolds number ratio  $Re_z/Re_x$ , as function of  $\theta_m$ , for  $Ra = 10^{10}$ : (a)  $\theta_m = 0.93$ , (b)  $\theta_m = 0.945$ , (c)  $\theta_m = 0.955$ . (d–g) Instantaneous temperature fields for different  $\theta_m$  at different times denoted by dashed lines in panels (b, c): (d)  $\theta_m = 0.945$ ,  $t/t_f = 1.5 \times 10^5$ ; (e)  $\theta_m = 0.945$ ,  $t/t_f = 1.8 \times 10^5$ ; (f)  $\theta_m = 0.955$ ,  $t/t_f = 1.1 \times 10^5$  and (g)  $\theta_m = 0.955$ ,  $t/t_f = 2.4 \times 10^5$ .

seen in Fig. 3(b).

Finally, we address the (rare) transitions between different flow states for large  $\theta_m$ . It was found that the Reynolds number ratio  $Re_z/Re_x$  can well differentiate different convection roll states [21, 22]. Here  $Re_z = \langle w^2 \rangle_{V,t}^{1/2} H/\nu$  is the volume averaged vertical Reynolds number and  $Re_x = \langle u^2 \rangle_{V,t}^{1/2} H/\nu$  the horizontal one. The Reynolds number ratios  $Re_z/Re_x$  for  $Ra = 10^{10}$  with large  $\theta_m$  close to  $\theta_m = 1$  are displayed in Fig. 4(a). The statistically stable two-roll state, as shown in Fig. 1(b), can be found for up to  $\theta_m = 0.93$ . However, once  $\theta_m$  increases to  $\theta_m = 0.945$ , the

two-roll state is not sustained all the time and rare transitions between two-roll and four-roll states occur, which can be seen in the rare jumps of the Reynolds number ratio  $Re_z/Re_x$  in Fig. 4(b). The temperature fields for the two-roll and four-roll states are shown in Figs. 4(d) and 4(e), respectively. At even larger  $\theta_m = 0.955$ , constant jumps between different states are observed, as displayed in Fig. 4(c). The instantaneous temperature fields at two instants are shown in Figs. 4(f) and 4(g). It can be seen that the convection rolls are now not well organised. When  $\theta_m$  reaches 0.97, the flow enters into the conduction state without any fluid motions.

Rare transitions between different turbulent states have been reported for many different flows [34–37]. Similar phenomena are also important in many geophysical flows [38, 39]. Here we have thus found another example of such rare transition events in turbulent flows, which were not identified for OB cases [21]. Similar to prior studies [36, 37], such phenomenon can be viewed as flow mode competition between different states: for not very large  $\theta_m$ , e.g.,  $\theta_m = 0.93$ , the effective aspect ratio of the convection region is close to  $\Gamma = 2$ , therefore, it only supports a two-roll state. At large  $\theta_m$  close to  $\theta_m = 1$ , the effective aspect ratio becomes much larger than 1, and therefore it can support more convection rolls [21]. In between, the different convection roll states may have comparable strength, and the competition of these states leads to the rare transitions between them.

In conclusion, based on our DNS of turbulent penetrative RBC in cold water, where the density anomaly temperature is achieved in the cell’s bulk, we have shown that the main response parameters, namely the mean central temperature  $\theta_c$  and the normalized Nusselt number, are universally determined by the density inversion parameter  $\theta_m$ . For  $\theta_m = 0$ , the convective system is similar to that in the Oberbeck-Boussinesq case. However, for  $\theta_m$  approaching 1, the convection vanishes at a certain  $\theta_m = \theta_{m,c}$  as soon as the Rayleigh number of the lower layer achieves the critical Rayleigh number  $Ra_c$  for the onset of convection. We have demonstrated that  $Ra_c$  and hence  $\theta_{m,c}$  can be excellently predicted by a linear stability analysis. We have further shown that in the range  $0 \leq \theta_m \lesssim \theta_{m,c}$ , the central temperature  $\theta_c(\theta_m)$  is independent of  $Ra$  and can be excellently predicted by our model. Furthermore, we proposed a theoretical model for the normalized heat transport.

Our theoretical results on the similarity of the bulk temperature and normalized heat transport in penetrative thermal convection and the observation of the rare transitions between the flow states are supported by the DNS data. They are relevant and important for numerous geophysical, astrophysical and engineering applications. Our approach of theoretically determining the response

parameters of penetrative convective turbulence in cold water around  $4^\circ$  may be transferred to other cases of penetrative convective turbulence.

*Acknowledgement:* R. Verzicco is gratefully acknowledged for continuous collaborations and discussions. We also acknowledge the Twente Max-Planck Center and the Deutsche Forschungsgemeinschaft (Priority Programme SPP 1881 "Turbulent Superstructures" and grant Sh405/10). The simulations were carried out on the national e-infrastructure of SURFsara, a subsidiary of SURF cooperation, the collaborative ICT organization for Dutch education and research. Q.W. acknowledges financial support from the China Scholarship Council (CSC) and the Natural Science Foundation of China (NSFC) under grant no. 11621202.

- 
- [1] G. Ahlers, S. Grossmann, and D. Lohse, "Heat transfer and large scale dynamics in turbulent Rayleigh-Bénard convection," *Rev. Mod. Phys.* **81**, 503–537 (2009).
  - [2] D. Lohse and K.-Q. Xia, "Small-scale properties of turbulent Rayleigh-Bénard convection," *Annu. Rev. Fluid Mech.* **42**, 335–364 (2010).
  - [3] F. Chillà and J. Schumacher, "New perspectives in turbulent Rayleigh-Bénard convection," *Eur. Phys. J. E* **35**, 58 (2012).
  - [4] J. M. Dumore, H. J. Merk, and J. A. Prins, "Heat transfer from water to ice by thermal convection," *Nature* **172**, 460–461 (1953).
  - [5] V. P. Carey, B. Gebhart, and J. C. Mollendorf, "Buoyancy force reversals in vertical natural convection flows in cold water," *J. Fluid Mech.* **97**, 279–297 (1980).
  - [6] V. P. Carey and B. Gebhart, "Visualization of the flow adjacent to a vertical ice surface melting in cold pure water," *J. Fluid Mech.* **107**, 37–55 (1981).
  - [7] Z. Wang, E. Calzavarini, C. Sun, and F. Toschi, "How the growth of lake ice depends on the fluid dynamics underneath," arXiv:2007.14252 (2020).
  - [8] George Veronis, "Penetrative convection," *Astrophys. J.* **137**, 641 (1963).
  - [9] Steven Musman, "Penetrative convection," *J. Fluid Mech.* **31**, 343–360 (1968).
  - [10] B. Dintrans, A. Brandenburg, Å. Nordlund, and R. F. Stein, "Spectrum and amplitudes of internal gravity waves excited by penetrative convection in solar-type stars," *Astron. Astrophys.* **438**, 365–376 (2005).
  - [11] B. Buffett, "Geomagnetic fluctuations reveal stable stratification at the top of the Earth's core," *Nature*

- 507**, 484–487 (2014).
- [12] K. Zhang and G. Schubert, “Penetrative convection and zonal flow on jupiter,” *Science* **273**, 941 (1996).
- [13] Benjamin Gebhart and Joseph C Mollendorf, “A new density relation for pure and saline water,” *Deep-Sea Res.* **24**, 831–848 (1977).
- [14] D. R. Moore and N. O. Weiss, “Nonlinear penetrative convection,” *J. Fluid Mech.* **61**, 553–581 (1973).
- [15] R. W. Walden and G. Ahlers, “Non-Boussinesq and penetrative convection in a cylindrical cell,” *J. Fluid Mech.* **109**, 89–114 (1981).
- [16] E Large and CD Andereck, “Penetrative Rayleigh-Bénard convection in water near its maximum density point,” *Phys. Fluids* **26**, 094101 (2014).
- [17] D. Lecoanet, M. Le Bars, K. J. Burns, G. M. Vasil, B. P. Brown, E. Quataert, and J. S. Oishi, “Numerical simulations of internal wave generation by convection in water,” *Phys. Rev. E* **91**, 063016 (2015).
- [18] Q. Wang, Q. Zhou, Z.-H. Wan, and D.-J. Sun, “Penetrative turbulent Rayleigh-Bénard convection in two and three dimensions,” *J. Fluid Mech.* **870**, 718–734 (2019).
- [19] R Verzicco and P Orlandi, “A finite-difference scheme for three-dimensional incompressible flows in cylindrical coordinates,” *J. Comput. Phys.* **123**, 402–414 (1996).
- [20] E. P. van der Poel, R. Ostilla-Mónico, J. Donners, and R. Verzicco, “A pencil distributed finite difference code for strongly turbulent wall-bounded flows,” *Comput. Fluids* **116**, 10–16 (2015).
- [21] Q. Wang, R. Verzicco, D. Lohse, and O. Shishkina, “Multiple states in turbulent large-aspect ratio thermal convection: What determines the number of convection rolls?” *Phys. Rev. Lett.* **125**, 074501 (2020).
- [22] Q. Wang, K.-L. Chong, R. J. A. M. Stevens, R. Verzicco, and D. Lohse, “From zonal flow to convection rolls in Rayleigh-Bénard convection with free-slip plates,” *J. Fluid. Mech.* **905**, A21 (2020).
- [23] O. Shishkina, R. J. A. M. Stevens, S. Grossmann, and D. Lohse, “Boundary layer structure in turbulent thermal convection and its consequences for the required numerical resolution,” *New J. Phys.* **12**, 075022 (2010).
- [24] D. Goluskin and E. P. van der Poel, “Penetrative internally heated convection in two and three dimensions,” *J. Fluid Mech.* **791**, R6 (2016).
- [25] D. Goluskin, *Internally heated convection and Rayleigh-Bénard convection* (Springer, 2016).
- [26] Q. Wang, O. Shishkina, and D. Lohse, “Scaling in internally heated convection: a unifying theory,”

- Geophys. Res. Lett.(In press),arXiv:2010.05789 (2020).
- [27] O. Shishkina, S. Grossmann, and D. Lohse, “Heat and momentum transport scalings in horizontal convection,” *Geophys. Res. Lett.* **43**, 1219–1225 (2016).
- [28] O. Shishkina and S. Wagner, “Prandtl-number dependence of heat transport in laminar horizontal convection,” *Phys. Rev. Lett.* **116**, 024302 (2016).
- [29] P. Reiter and O. Shishkina, “Classical and symmetrical horizontal convection: detaching plumes and oscillations,” *J. Fluid Mech.* **892**, R1 (2020).
- [30] D. P. M. Van Gils, S. G. Huisman, G.-W. Bruggert, C. Sun, and D. Lohse, “Torque scaling in turbulent Taylor-Couette flow with co-and counterrotating cylinders,” *Phys. Rev. Lett.* **106**, 024502 (2011).
- [31] R. Ostilla-Mónico, R. J. A. M Stevens, S. Grossmann, R. Verzicco, and D. Lohse, “Optimal Taylor–Couette flow: direct numerical simulations,” *J. Fluid Mech.* **719**, 14–46 (2013).
- [32] R. Ostilla-Mónico, E. P. van der Poel, R. Verzicco, S. Grossmann, and D. Lohse, “Exploring the phase diagram of fully turbulent Taylor–Couette flow,” *J. Fluid Mech.* **761**, 1–26 (2014).
- [33] E. P. van der Poel, R. J. A. M. Stevens, and D. Lohse, “Comparison between two-and three-dimensional Rayleigh–Bénard convection,” *J. Fluid Mech.* **736**, 177–194 (2013).
- [34] K. Sugiyama, R. Ni, R. J. A. M. Stevens, T. S. Chan, S.-Q. Zhou, H.-D. Xi, C. Sun, S. Grossmann, K.-Q. Xia, and D. Lohse, “Flow reversals in thermally driven turbulence,” *Phys. Rev. Lett.* **105**, 034503 (2010).
- [35] E. P. van der Poel, R. J. A. M Stevens, and D. Lohse, “Connecting flow structures and heat flux in turbulent Rayleigh–Bénard convection,” *Phys. Rev. E* **84**, 045303 (2011).
- [36] Y.-C. Xie, G.Y. Ding, and K.-Q. Xia, “Flow topology transition via global bifurcation in thermally driven turbulence,” *Phys. Rev. Lett.* **120**, 214501 (2018).
- [37] Q. Wang, Z.-H. Wan, R. Yan, and D.-J. Sun, “Multiple states and heat transfer in two-dimensional tilted convection with large aspect ratios,” *Phys. Rev. Fluids* **3**, 113503 (2018).
- [38] G. A. Glatzmaier and P. H. Roberts, “A three-dimensional self-consistent computer simulation of a geomagnetic field reversal,” *Nature* **377**, 203–209 (1995).
- [39] E. R. Weeks, Y. Tian, J. S. Urbach, K. Ide, H. L. Swinney, and M. Ghil, “Transitions between blocked and zonal flows in a rotating annulus with topography,” *Science* **278**, 1598–1601 (1997).